PASJ: Publ. Astron. Soc. Japan **46**, 629–642 (1994)

Spectral Evolution of the H_2O Maser in Late-Type Stars

Hiroshi TAKABA
Communications Research Laboratory, Kashima Space Research Center 893-1 Hirai, Kashima, Ibaraki 314

Nobuharu UKITA and Takeshi MIYAJI
Nobeyama Radio Observatory, Minamisaku, Nagano 384-13
and
Makoto MIYOSHI
National Astronomical Observatory at Mizusawa, Hoshigaoka, Mizusawa, Iwate 023

(Received 1994 January 24; accepted 1994 September 8)

Abstract

We have carried out almost simultaneous observations of H_2O and SiO ($J = 1$–0, $v = 1$) masers for 171 known late-type maser stars with the 34 m radio telescope at Kashima. We found a systematic change in the H_2O maser spectra related to the evolution of the stars. Typically, H_2O maser spectral profiles are singly peaked in Mira variables, but doubly peaked in IRC/AFGL objects and OH/IR stars. The expansion velocity of H_2O masers increases with decreasing IRAS color temperature. This is explained by the shock excitation model proposed by Cooke and Elitzur (1985, AAA 40.064.014). The blue shifted peak in the profiles is more prominent than the red shifted peak in most of the IRC/AFGL objects and OH/IR stars. A blocking model of the redshifted peak is introduced.

Key words: Circumstellar matter — Masers — Stars: circumstellar shells — Stars: late-type — Stars: variable

1. Introduction

Far-infrared observations by the Infrared Astronomical Satellite (IRAS) and radio observations of masers have provided new information about the circumstellar dust/gas envelopes in late-type stars. In particular, thousands of intermediate-mass oxygen-rich M-type stars on the asymptotic giant branch (AGB) were detected by IRAS. Also, hundreds of masers have been found. As a result of these observations, it was found that M-type stars evolve in a sequence of Mira variables, IRC (or AFGL) objects, OH/IR stars, proto-planetary nebulae, and planetary nebulae. Using the IRAS database, Olnon et al. (1984), Bedjin (1987), and van der Veen and Habing (1988) investigated the characteristics of M-type stars. These studies show that these stars evolve on a narrow track in the IRAS two-color diagram (12/25 and 25/60 μm). This indicates that as a star evolves the circumstellar dust/gas envelope becomes dense and the IRAS color temperature decreases. Further, when the mass loss stops, stars evolve to proto-planetary nebula and finally to the planetary nebula.

Three molecules, OH, H_2O, and SiO, exhibit strong masers in M-type stars. SiO masers need the highest temperature for pumping and are emitted from the region closest to the central star. OH molecules are produced by the photo-dissociation process of the H_2O molecules, and OH masers are emitted from the outer region of circumstellar envelopes. The H_2O maser is emitted from the area between the SiO and OH masers (e.g., Reid, Moran 1981).

Typical OH 1612 MHz masers have doubly peaked emission which is thought to be emitted from an expanding circumstellar shell (Reid et al. 1977). Based on an OH-maser calculation, Netzer and Knapp (1987) showed that the mass-loss rates are in the range from $10^{-7} M_\odot$ yr^{-1} to $10^{-6} M_\odot$ yr^{-1} for Mira variables, from 10^{-6} to $10^{-5} M_\odot$ yr^{-1} for IRC/AFGL objects, and from 10^{-5} to $10^{-4} M_\odot$ yr^{-1} for OH/IR stars. Dickinson and Kleinmann (1977) show that some H_2O masers also have doubly peaked emission with velocities that are slightly less than that of OH masers.

Some masers change their intensities in phase with the optical and near-infrared intensity variations (Schwartz et al. 1974 for H_2O masers). Therefore, simultaneous observations are necessary for a direct comparison of the different types of maser transitions. Such observations have not been conducted before. The new 34 m radio telescope of the Communications Research Laboratory (CRL) has receivers from the 1.6 GHz to the 43 GHz band, most of the stellar and interstellar maser transitions within this frequency range are observable.

In order to produce a database of the stellar maser sources and to carry out a statistical study of stellar

masers, we have carried out a snapshot survey of H_2O and SiO(J = 1–0, v = 1) masers using the 34-m radio telescope at Kashima. In this paper we discuss the correlation of the H_2O and SiO maser profiles with the position of the IRAS color-color diagram.

2. Observations

The observations were made during 1991 from April 26 to May 11 with the 34 m telescope of the Kashima Space Research Center, Communications Research Laboratory, Japan. Details conserning the telescope system have been described by Takaba (1991). The telescope was equipped with a 43 GHz band HEMT receiver developed by Nobeyama Radio Observatory (NRO) and a 22 GHz band HEMT receiver developed by National Radio Astronomy Observatory (NRAO). Both of the receivers are cryogenically cooled to 15 K by closed-cycle gas-helium refrigerators. The single side-band system noise temperature including the sky at the zenith was about 900 K for the SiO J = 1–0, v = 1 transition at 43.122 GHz and 180 K for the H_2O 6_{16}–5_{23} transition at 22.235 GHz. The aperture efficiencies were 40% and 57% at the 43 GHz and 22 GHz band, respectively.

A portable acousto-optical spectrometer (AOS) using an optical diode-laser which was developed by NRO was used for the observations at Kashima. The bandwidth of the specrometer 40 MHz and the frequency resolution 40 kHz, results in a velocity resolution of 0.35 km s^{-1} at 43 GHz and 0.7 km s^{-1} at 22 GHz. For the 22 GHz band receiver, a room-temperature hot load was used to calibrate the intensity of the H_2O masers. Under cloudy conditions, the absolute intensity in the H_2O maser data is considered to be accurate within 30%. Though the 43 GHz band receiver did not have calibration equipment at the time of the observation, the system was very stable and the maser intensity was checked for one day under clear-sky conditions. The error in the intensity scale is estimated to be about 20% for the standard calibration sources. For the 43 GHz SiO masers, we adopted peak intensities of 1600 Jy (for -6 km s^{-1} component), 1500 Jy, and 900 Jy for Orion KL, VY CMa, and R Leo, respectively.

The sources were mainly chosen from the catalog of stellar maser sources by Benson et al. (1990). We selected most of the sources in which SiO and OH/H_2O were detected. Table 1 summarizes the observational results; it contains 206 sources, 171 of which were observed both in H_2O and SiO. The observations were made in the SiO J = 1–0, v = 1 transition at 43 GHz during the period 1991 April 26–29; out of the 198 sources observed 75 were detected at more than 5-σ noise level. Regarding H_2O transition at 22 GHz during the period 1991 May 10–11, 179 sources were observed and 87 sources were detected. All of the observations were made in the position-switching mode. The integration time was typically 10–15 min for each observation; and the rms noise level was 1 Jy in SiO and 0.2 Jy in H_2O for a resolution of 40 kHz.

3. Results

Table 1 lists the observed results, and the profiles for both H_2O and SiO emission are shown in figure 1. A Gaussian fitting was made in order to obtain the central velocity and width for singly peaked sources and sources with blended components. For doubly peaked sources, a Gaussian fitting was made separately for each peak. The maser catalog by Benson et al. (1990) contains some interstellar maser sources. We have excluded the sources from our list for which the IRAS 2.5 log(F60/F25) is greater than 1.0 (for example, OH 205.1–14.1 and OH 12.22–0.12, both of which have a very strong H_2O maser) because they are in either the reflection nebula or the H II region, and are thought to be interstellar sources. Newly detected maser sources are T Ari, GL 5353, V1804 Sgr, and μ Cep in the H_2O maser, and SY Scl, IRC +60154, V697 Her, and BU And in the SiO maser. Although they are not listed in the catalog by Benson et al., the SiO masers in GL 5353 and V1804 Sgr were detected by Hall et al. (1990), and the SiO in MY Cep by Alcorea et al. (1990).

Figure 2 shows the IRAS color-color diagram of the sources with H_2O emission. The broken lines indicate the boundary of regions of II, IIIa, IIIb, and IV according to figure 5b of van der Veen and Habing (1988). Most of the region-II stars are Mira variables, the region-IIIa stars IRC/AFGL objects, and the region-IIIb and -IV stars OH/IR stars. Region II consists of O-rich variable stars with "young" circumstellar shells, IIIa more evolved circumstellar shells, IIIb thick circumstellar shells, and IV very thick circumstellar shells. Hereafter, we define these stars involved in the II, IIIa, IIIb, and IV regions Mira variables, IRC/AFGL objects, and OH/IR stars, respectively.

Figure 3 shows a plot of the H_2O maser velocity width versus the IRAS 25 and 12μm intensity ratio. We can see a correlation between the IRAS color and the H_2O velocity width.

For Mira variables, the mean velocity difference for the peaks between SiO J = 1–0, v = 1 and H_2O of $-0.86 +/- 3.0$ km s^{-1} (V_{H_2O}–V_{SiO}) were obtained from this observation.

For UX Cyg, the velocity differences between the H_2O and SiO peak velocities exceed the 2-σ value. In figure 2 (and figure 4), the position of UX Cyg is quite different from those of the Mira variables. These facts suggest that the kinematics in the dust/gas envelope of UX Cyg are different from those of the normal Mira. It is therefore supposed that H_2O and SiO masers must be emitted from different regions in the envelope because of the large

Table 1.

Name	Position						$H_2O(6_{16}$–$5_{23})$			SiO($J=1$–0, $v=1$)			IRAS color		Benson	
	R.A.(1950)			Decl.(1950)			S	V_{LSR}	ΔV	S	V_{LSR}	ΔV	[25–12]	[60–25]	H_2O	SiO
	h	m	s	°	′	″	Jy	km s^{-1}	km s^{-1}	Jy	km s^{-1}	km s^{-1}				
Y Cas	0	0	45.0	+ 55	24	21.0	4.6	−18.4	2.8	28.5	−15.9	3.1	−.80	−2.02	Y	Y
SV And	0	1	46.0	+ 39	49	54.0	<2			<9			−1.03	−2.06	N	Y
SY Scl	0	5	3.0	− 25	46	18.0	5.8	21.5	4.2	18.7	24.0	4.9	−.71	−2.17	Y	N
S Scl	0	12	51.0	− 32	19	24.0	<2			<15			−1.09	−1.86	Y	Y
T Cas	0	20	31.0	+ 55	30	54.0	<2			<7			−.95	−2.18	N	Y
R And	0	21	23.0	+ 38	18	.0	<2			<15			−.72	−2.12	N	Y
TY Cas	0	34	5.0	+ 62	51	30.0	3.7	−59.5	1.4	<7			−1.04	−2.34	Y	
V524 Cas	0	42	52.0	+ 68	55	.0	2.9	−26.4	22.1	<6			−.36	−1.80	Y	Y
WX Psc	1	3	48.0	+ 12	19	45.0	13.8	8.3	22.8	77.4	9.1	2.0	−.20	−1.63	Y	Y
IRC+30021	1	8	30.0	+ 30	22	.0	<2			<10			−.33	−2.04	Y	N
S Cas	1	15	58.0	+ 72	20	54.0	<2			6.6	−29.9	1.8	−.61	−2.17	N	Y
OH127.8-0.0	1	30	27.6	+ 62	11	31.2	<2			<10			.49	−.93	Y	Y
IRC+50049	1	55	35.0	+ 45	11	42.0	<2			<7			−.59	−2.10	Y	Y
R Ari	2	13	16.0	+ 24	49	30.0	<2			<8			−1.21		N	
W And	2	14	23.0	+ 44	4	30.0	<2			24.6	−34.8	1.8	−.91	−1.84	N	Y
o Cet	2	16	49.0	− 3	12	12.0	<2			<15			−.84	−2.19	Y	Y
S Per	2	19	15.1	+ 58	21	34.0	33.9	−37.6	17.7	22.0	−39.9	10.0	−.41	−1.91	Y	Y
R Cet	2	23	29.0	− 0	24	12.0	<2			<12			−.33	−1.89	Y	Y
RR Per	2	25	6.0	+ 51	2	54.0	<2			8.5	11.2	6.3	−.96	−1.87	N	Y
U Cet	2	31	20.0	− 13	22	1.0	<2			<14			−1.13	−1.90	Y	Y
IRC+60092	2	31	43.0	+ 64	56	36.0	<2			<6			−.46	−2.10	Y	
R Tri	2	34	.0	+ 34	2	50.0	<2			<12			−1.16	−1.96	Y	Y
IRC-30023	2	35	8.0	− 27	11	24.0	<2			<10			−.54	−2.18	Y	Y
RR Cep	2	36	12.0	+ 80	55	24.0	<2			<7			−.79	−2.06		
RU Ari	2	42	2.0	+ 12	6	30.0	4.0	19.4	1.8	<9			−.55	−1.76	Y	N
T Ari	2	45	32.0	+ 17	18	6.0	2.0	−4.3	1.5	<9			−1.01	−1.98	N	Y
U Ari	3	8	16.0	+ 14	36	48.0	<2			<11			−1.08	−1.83	N	Y
OH138.0+7.3	3	20	41.0	+ 65	21	31.0	<2			<8			.36	−1.39	N	Y
NML Tau	3	50	43.6	+ 11	15	32.0	63.3	33.7	23.2	244	34.7	3.5	−.72	−2.14	Y	Y
WZ Eri	3	59	50.0	− 13	53	18.0	<2			14.5	6.9	2.5	−.78	−2.10	Y	
TZ Tau	3	59	55.0	+ 16	32	18.0	<2			<9			−1.05			
V Eri	4	2	2.0	− 15	51	42.0	<2			<15			−.62	−2.24	N	Y
W Eri	4	9	26.0	− 25	15	42.0	19.6	−0.4	1.1	30.9	−0.3	2.6	−.90	−2.15	Y	Y
R Tau	4	25	33.3	+ 10	3	16.0	<2			15.2	13.5	1.3	−.72	−1.95	Y	Y
S Tau	4	26	27.0	+ 9	50	12.0	<2			<15			−1.02	−1.99	N	Y
BD Eri	4	31	10.0	− 0	5	.0	<2			<11			−.91	−2.11	Y	
RX Tau	4	35	32.0	+ 8	14	12.0	<2			16.3	−41.0	5.0	−.93	−2.04	Y	Y
R Cae	4	38	46.0	− 38	19	54.0	-			23.4	−1.6	2.1	−.93	−2.15	Y	Y
TX Cam	4	56	44.0	+ 56	6	54.0	<2			10.0	9.0	2.6	−1.03	−1.69	N	Y
T Lep	5	2	43.2	− 21	58	19.0	4.2	−27.4	4.0	38.2	−27.2	1.7	−.70	−2.12	Y	Y
IRC+50137	5	7	19.7	+ 52	48	53.0	1.6	3.2	18.6	20.6	4.4	3.9	.20	−1.45	Y	Y
R Aur	5	13	15.0	+ 53	31	54.0	<2			10.2	−2.6	5.0	−1.00	−2.28	N	Y
IRC+60154	5	15	5.0	+ 63	12	54.0	6.8	52.3	16.0	19.3	48.1	3.5	−.70	−2.08	Y	N
T Col	5	17	27.0	− 33	45	30.0	<2			14.6	−36.1	4.0	−1.06	−2.13	N	Y
S Ori	5	26	32.7	− 4	43	52.0	<2			<15			−.94	−1.81	N	Y
BK Ori	5	29	13.0	− 7	24	.0	<2			<15						Y
RW Lep	5	36	37.0	− 14	3	48.0	2.2	−60.2	5.0	<10			−.88	−1.76	Y	
RU Aur	5	36	43.0	+ 37	36	36.0	<2			14.3	−31.4	5.9	−.70	−2.12	N	Y
U Aur	5	38	55.0	+ 32	1	6.0	<2			<8			−.81	−1.73	Y	Y
IRC+70066	5	41	16.0	+ 69	56	54.0	21.5	−10.2	4.2	5.4	−1.7	5.8	−.74	−2.24	Y	Y
AW Tau	5	44	20.0	+ 27	6	32.0	15.7	−11.7	3.1	<6			−.81	−2.10	Y	N
U Ori	5	52	51.0	+ 20	10	6.0	26.5	−37.5	1.1	53.0	−41.6	3.1	−1.05	−2.06	Y	Y

Table 1. (continued)

Name	Position R.A.(1950) h m s	Decl.(1950) ° ′ ″	$H_2O(6_{16}–5_{23})$ S Jy	V_{LSR} km s^{-1}	Δ V km s^{-1}	SiO($J=1$–0, $v=1$) S Jy	V_{LSR} km s^{-1}	Δ V km s^{-1}	IRAS color [25–12]	[60–25]	Benson H_2O	SiO
V Cam	5 55 58.0	+ 74 30 24.0	<2			12.4	6.1	7.0	−.71	−1.97	Y	Y
GI Ori	6 10 25.0	+ 18 33 30.0	<2			<9			−.90	−1.76	N	
V Mon	6 20 12.0	− 2 10 12.0	<2			<9			−1.16	−1.72	N	Y
IRC+40156	6 29 45.0	+ 40 44 54.0	<2			9.5	−18.5	4.0	−.09	−1.66	Y	Y
IRC+60169	6 30 .6	+ 60 58 54.0	116	−27.2	13.2	32.6	−22.8	5.1	−.36	-1.68	Y	Y
SY Mon	6 34 59.0	− 1 20 42.0	7.3	−56.9	1.1	21.7	−54.5	1.5	−.79	−1.90	Y	Y
U Lyn	6 36 19.0	+ 59 54 48.0	3.8	−14.4	7.7	<6			−.92	−2.18	Y	Y
S Lyn	6 40 15.0	+ 57 57 42.0	<2			<6			−1.00	−1.90	N	Y
FX Mon	6 42 21.0	+ 9 5 24.0	<2			<7			−.84	−2.30	N	
X Gem	6 43 55.0	+ 30 19 54.0	<2			<7			−1.30	−2.12	N	Y
GX Mon	6 49 59.0	+ 8 29 6.0	<2			<9			−.56	−1.33	Y	Y
IRC-10151	7 5 26.0	− 10 39 30.0	6.7	50.1	10.6	-			−.31	−2.02	Y	Y
AFGL1099	7 15 14.0	− 34 44 42.0	-			<12			−.70	−2.23	N	Y
VY CMa	7 20 54.6	− 25 40 12.5	1980	16.9	3.8	1080	22.6	2.8	−.43	−1.65	Y	Y
Z Pup	7 30 29.0	− 20 32 48.0	-			16.3	1.9	5.3	−.75	−1.91	Y	Y
IRC+30187	7 30 44.0	+ 30 37 12.0	85.0	5.5	23.0	<7			−.67	−2.37	Y	
QX Pup	7 39 59.0	− 14 35 44.0	-			<8			2.69	.96	Y	Y
R Cnc	8 13 48.5	+ 11 52 50.0	2.7	14.3	2.9	7.6	13.6	2.3	−1.07	−1.96	Y	Y
OH235.3+18	8 35 44.5	− 10 13 40.0	2.2	65.0	2.0	-			−.06	−1.88	Y	N
S Hya	8 50 57.0	+ 3 15 30.0	<2			<8			−1.20	−1.89	N	Y
IRC-20176	8 53 25.0	− 19 1 42.0	12.2	7.0	1.4	<9			−.71	−2.07	Y	
W Cnc	9 6 58.0	+ 25 27 6.0	<2			<12			−.74	−1.91	Y	Y
IRC-20188	9 23 35.0	− 23 47 38.0	-			26.0	11.4	3.2	−.36	−1.65	Y	Y
X Hya	9 33 6.0	− 14 28 1.9	6.0	26.0	4.0	10.8	23.7	10.2	−1.01	−2.14	Y	Y
R LMi	9 42 34.7	+ 34 44 34.3	9.7	0.1	2.9	28.7	0.0	6.0	−.96	−2.09	Y	Y
R Leo	9 44 52.2	+ 11 39 40.0	<2			829	−.19	2.2	−1.30	−1.90	Y	Y
CW Leo	9 45 15.0	+ 13 30 42.0	<2			<9			−.78	−1.53	N	Y
S LMi	9 50 45.0	+ 35 9 42.0	<2			<7			−.91	−1.53	Y	Y
RW LMi	10 13 12.0	+ 30 49 24.0	<2			<11			−1.09	−1.62	N	Y
V Ant	10 18 55.0	− 34 32 48.0	-			<15			−.56	−2.24	Y	Y
R UMa	10 41 8.0	+ 69 2 18.0	8.8	43.5	9.2	32.6	39.2	2.9	−.59	−2.24	Y	Y
W Leo	10 50 59.0	− 13 58 54.0	2.7	45.4	4.2	11.1	46.2	3.7			Y	Y
R Crt	10 58 6.0	− 18 3 21.0	192	8.6	12.9	15.9	8.0	3.6	−.79	−1.99	Y	Y
AF Leo	11 25 17.0	+ 15 26 .0	<2			<6			−.48	−2.26	Y	
S Crt	11 50 12.0	− 7 19 6.0	82.3	38.0	4.2	<9			−.93	−1.88	Y	N
R Com	12 1 42.0	+ 19 3 42.0	<2			<8			−.69	−1.72	Y	Y
T Vir	12 12 3.0	− 5 45 30.0	4.3	7.4	1.9	<9			−.61	−1.85	Y	Y
T UMa	12 34 7.0	+ 59 45 42.0	<2			<10			−.95	−1.70	Y	Y
R Vir	12 35 58.0	+ 7 15 48.0	<2			<9			−1.13	−1.93	N	Y
U Cvn	12 44 56.0	+ 38 38 54.0	-			<10			−.44	−2.18	Y	N
T Com	12 56 13.0	+ 23 24 36.0	6.9	26.7	3.3	<8			−.58	−1.85	Y	N
RT Vir	13 0 5.7	+ 5 27 22.0	-			<10			−.78	−1.91	Y	Y
R Hya	13 26 59.0	− 23 1 30.0	-			29.0	−10.9	7.8	−1.09	−2.04	Y	Y
S Vir	13 30 23.0	− 6 56 24.0	-			19.1	12.4	10.0	−.98	−2.07	Y	Y
T UMi	13 33 39.0	+ 73 41 12.0	<2			<10			−1.07	−2.20	Y	N
W Hya	13 46 12.1	− 28 7 8.5	-			368	40.5	6.9	−1.37	−1.96	Y	Y
R Cvn	13 46 49.0	+ 39 47 24.0	-			<8			−1.01	−2.06	Y	Y
AY Vir	13 49 16.0	− 3 25 48.0	-			<10			−.82	−1.91	Y	N
Z Boo	14 4 4.0	+ 13 43 18.0	-			<10			−.93		Y	N
RU Hya	14 8 41.0	− 28 39 .0	-			<10			−.75	−1.87	Y	N
U UMi	14 16 14.0	+ 67 1 30.0	<2			<8			−.98	−2.18	N	Y
RX Boo	14 21 56.6	+ 25 55 50.0	-			<7			−.76	−1.96	Y	Y

Table 1. (continued)

Name	Position						$H_2O(6_{16}-5_{23})$			$SiO(J=1-0, v=1)$			IRAS color		Benson	
	R.A.(1950)			Decl.(1950)			S	V_{LSR}	ΔV	S	V_{LSR}	ΔV	[25–12]	[60–25]		
	h	m	s	°	′	″	Jy	km s^{-1}	km s^{-1}	Jy	km s^{-1}	km s^{-1}			H_2O	SiO
RS Vir	14	24	46.0	+	4	54	9.0	54.3	−14.9	1.7	19.4	−10.8	3.2	−.56	−1.87	Y	Y
15060+0947	15	6	.0	+	9	47	43.0	-			<7			--.30	−2.08	Y	
Y Lib	15	9	3.0	−	5	49	24.0	-			<9			−.74	−2.05	Y	
S Ser	15	19	19.0	+	14	29	36.0	17.5	21.9	3.9	13.3	21.4	6.0	−.93	−1.30	Y	Y
S Crb	15	19	21.3	+	31	32	46.0	21.9	1.0	1.6	15.5	0.5	3.3	−.51	−2.05	Y	Y
RS Lib	15	21	24.0	−	22	44	.0	-			19.9	5.0	6.3	−1.14	−1.87	N	Y
WX Ser	15	25	32.0	+	19	44	6.0	3.1	7.7	1.5	<9			−.49	−2.30	Y	Y
IRC+00266	15	26	17.0	+	3	59	42.0	-			<9			−.44	−2.06	Y	N
WW Ser	15	29	55.0	+	3	48	42.0	-			<11			−.91	−2.30	Y	
S UMi	15	31	27.0	+	78	48	6.0	<2			<10			−.99	−2.25	N	Y
R Ser	15	48	23.0	+	15	17	6.0	-			48.5	33.6	1.9	−1.07	−2.01	Y	Y
FS Lib	15	57	37.0	−	12	12	36.0	-			<15			−.54	−1.88	Y	
RU Her	16	8	8.0	+	25	11	59.0	<2			<12			−.86	−2.11	N	Y
U Her	16	23	34.9	+	19	0	16.0	45.9	−16.1	5.7	31.4	−15.8	9.1	−1.11	-2.06	Y	Y
V697 Her	16	25	59.9	+	34	54	36.0	<2			15.3	55.2	4.6	−.25	−1.73	Y	N
R UMi	16	30	38.0	+	72	23	12.0	5.3	−8.2	2.2	<11			−.93	−2.03	Y	Y
T Oph	16	30	52.0	−	16	1	36.0	-			18.9	−29.7	3.4	−.92	−1.80	N	Y
RX Oph	16	50	20.0	+	5	29	24.0	9.2	−48.6	1.1	-			−.68	−1.95	Y	N
RR Sco	16	53	26.3	−	30	30	9.1	<2			17.5	−26.9	3.2	−1.07	−1.94	N	Y
MV Her	16	56	3.0	+	22	52	36.0	<2			<9			−.61	−1.80	Y	
V850 Oph	17	3	24.0	−	10	25	1.6	2.5	1.3	2.0	<14			−.54	−2.03	Y	
R Oph	17	4	53.0	−	16	1	42.0	<2			<11			−1.13	−1.93	N	Y
VV Her	17	5	3.0	+	17	14	12.0	1.5	−78.4	2.1	-			−.54	−1.94	Y	
AH Sco	17	8	2.0	−	32	15	52.6	71.0	−3.0	9.0	53.3	−0.3	6.5	−.64	−1.70	Y	Y
IRC+10322	17	11	56.0	+	8	59	18.0	8.0	12.6	13.7	32.0	13.1	3.0	−.40	−2.23	Y	Y
17230+0113	17	23	4.0	+	1	13	39.0	3.3	−30.8	9.7	<8			−.17	−1.86	Y	
IRC+103293	17	25	40.0	+	5	5	36.0	-			<10			−.20	−1.54	Y	N
GL5353	17	30	58.2	−	17	24	19.0	3.3	64.3	8.5	15.2	56.4	5.4	−.31	−2.61		
GL5357	17	32	53.6	−	33	27	50.0	1.5	−15.8	2.2	<15			−.34	−1.13	Y	
IRC-30308	17	35	27.0	−	31	55	48.0	15.2	1.9	7.3	<12			−.22		Y	Y
OH358.23+0.11	17	37	40.0	−	30	21	39.0	26.3	−6.8	10.0	<9			−.37	−1.56	Y	
OH358.67-0.04	17	39	20.0	−	30	4	19.0	16.8	−16.1	16.8	<9			−.17		Y	
V2211 Oph	17	48	28.0	−	8	0	42.0	10.2	−22.0	1.5	<9			−.47	−2.21	Y	Y
OH2.58-0.43	17	50	11.0	−	26	56	1.0	2.8	−7.5	21.8	38.2	−1.5	5.2	−.24		Y	Y
RT Oph	17	54	11.3	+	11	10	30.0	1.6	−18.6	2.6	11.8	−14.0	3.7	−.85	−1.97	Y	Y
IRC-20424	18	0	58.0	−	20	19	12.0	1.9	8.8	12.3	18.0	14.7	1.0	−.38	-2.01	Y	Y
V1804 Sgr	18	1	52.6	−	28	2	10.0	20.9	24.3	1.8	17.3	29.5	1.7	−.60	-1.87		
IRC-20427	18	2	38.0	−	21	14	.0	19.2	8.1	20.4	<7			−.17	−1.50	Y	
VX Sgr	18	5	2.9	−	22	13	56.0	184	−0.3	12.7	46.7	9.1	10.7	−7.4	−1.81	Y	Y
OH10.1-0.1	18	5	17.0	−	20	16	37.0	<2			<10			.45	1.01	Y	
T Her	18	7	13.0	+	31	0	42.0	<2			<8			−1.07	−1.78	N	Y
18076+3445	18	7	37.0	+	34	45	40.0	3.0	12.8	3.3	<7			−.18	−1.80	Y	Y
GL2086	18	8	18.8	−	26	30	14.0	<2			<10			.25	−2.01		
OH15.68+0.8	18	13	26.0	−	14	56	34.0	<2			<9			1.50	.26	Y	Y
IRC-20454	18	13	31.0	−	16	41	2.0	46.3	48.3	14.4	16.4	44.6	12.1	−.44		Y	Y
RY Oph	18	14	7.0	+	3	40	24.0	<2			<8			−1.08	−1.47	N	Y
OH12.8-1.9	18	17	40.0	−	18	48	31.0	29.5	10.3	33.3	29.0	10.3	3.9	.41	-1.34	Y	Y
OH16.12-0.29	18	18	15.0	−	15	4	48.0	<2			<9			1.04	.22	Y	Y
IRC-10414	18	20	28.0	−	13	44	6.0	32.6	39.8	15.1	16.8	40.7	4.6	−.46	1.62	Y	Y
V434 Sct	18	25	26.0	−	11	18	6.0	<2			<9			.37		Y	Y
OH24.7+0.2	18	32	47.0	−	7	15	37.0	11.1	43.5	32.7	17.8	43.6	1.5	.66	.17	Y	Y

Table 1. (continued)

Name	Position R.A.(1950) h m s	Decl.(1950) ° ′ ″	$H_2O(6_{16}–5_{23})$ S Jy	V_{LSR} km s^{-1}	ΔV km s^{-1}	SiO($J=1$–0, $v=1$) S Jy	V_{LSR} km s^{-1}	ΔV km s^{-1}	IRAS color [25–12]	[60–25]	Benson H_2O	SiO
OH26.5+0.5	18 34 52.0	− 5 26 36.0	12.2	25.8	18.1	<8			.61	−.34	Y	Y
V1111 Oph	18 34 57.7	+ 10 23 5.0	32.4	−44.3	2.0	-			−.89	−1.72	Y	Y
X Oph	18 35 57.4	+ 8 47 20.0	4.1	−56.0	1.9	-			−1.12	−2.04	Y	Y
V438 Sct	18 38 32.0	− 6 18 6.0	7.7	55.3	2.8	<10			.43		Y	Y
IRC+10374	18 41 17.0	+ 13 54 30.0	5.1	−14.8	13.0	22.0	−18.0	4.3	−.43	−2.13	Y	Y
S Sct	18 47 37.1	− 7 57 59.0	<2			<8			−1.44	−.69		
OH32.8-0.3	18 49 48.2	− 0 17 53.0	<2			<7			1.15		Y	Y
OH39.7+1.5	18 56 3.9	+ 6 38 49.8	4.9	25.7	16.5	33.1	22.3	1.5	.21	−1.29	Y	Y
R Aql	19 3 57.7	+ 8 9 10.3	19.5	47.6	3.1	40.9	47.0	1.8	−.54		Y	Y
U Dra	19 9 58.0	+ 67 11 36.0	<2			<11			−1.02	−1.96	Y	Y
RU Lyr	19 10 43.0	+ 41 13 6.0	<2			<9			−.90	−2.38	Y	
RT Aql	19 35 40.0	+ 11 36 24.0	27.9	−30.2	1.5	<12			−.81	−1.84	Y	Y
χ Cyg	19 48 38.5	+ 32 47 11.0	<2			<15			−1.42	−1.89	N	Y
RR Sgr	19 52 49.9	− 29 19 23.9	-			<10			−1.05	−2.10	Y	Y
RR Aql	10 55 .3	− 2 1 17.1	114	27.9	1.6	53.6	26.0	2.8	−.86	−1.86	Y	Y
Z Cyg	20 0 2.0	+ 49 54 12.0	<2			<11			−2.1	−2.01	Y	Y
SY Aql	20 4 45.0	+ 12 48 24.0	41.8	−47.6	1.9	-			−.75	−2.02	Y	Y
R Del	20 12 30.0	+ 8 56 6.0	3.6	−31.9	1.3	-			−1.05	−2.04	Y	Y
20171+2732	20 17 6.0	+ 27 32 42.0	<2			<8			−.07	−1.61	Y	
KY Cyg	20 24 6.0	+ 38 11 18.0	<2			<12			−.48	−2.04	Y	Y
20246+2813	20 24 41.0	+ 28 13 58.0	<2			<8			−.17	−2.14	Y	
DR Cyg	20 41 47.0	+ 37 48 24.0	<2			<9					Y	
NML Cyg	20 44 33.8	+ 39 55 57.0	38.3	5.0	49.9	<12					Y	Y
UX Cyg	20 53 .2	+ 30 13 20.0	36.1	−3.4	3.6	19.3	4.1	8.3	−.58	−.91	Y	Y
μ Cep	21 41 58.7	+ 58 33 2.6	2.7	25.8	1.4	163	25.8	2.4	−.80	−.79	N	Y
TU Peg	21 42 39.0	+ 12 28 .0	29.9	10.5	1.5	19.4	12.3	4.1	−.87	−2.03	Y	Y
V Peg	21 58 32.0	+ 5 52 48.0	<2			<7			−1.10	−1.82	N	Y
TW Peg	22 1 43.0	+ 28 6 18.0	<2			<7			−.59	−2.13	Y	N
SV Peg	22 3 31.0	+ 35 6 18.0	14.2	7.4	7.7	<6			−.65	−1.99	Y	Y
IRC+10510	22 4 52.0	− 11 39 12.0	<2			<12					N	Y
RS Peg	22 9 50.0	− 14 18 24.0	<2			<10					N	Y
OH104.91+2	22 17 42.0	+ 59 36 17.0	3.1	−38.4	4.5	<6			.69	−1.10	Y	Y
RV Peg	22 23 20.0	+ 30 13 6.0	<2			<7			−.59	−2.11	N	Y
SS Peg	22 31 36.0	+ 24 18 18.0	<2			<9			−1.21	−2.01		Y
IRC+10523	22 51 40.0	+ 8 37 54.0	13.8	−2.5	2.9	20.5	3.3	6.0	−.62	−1.87	Y	Y
MY Cep	22 52 31.0	+ 60 33 18.0	12.5	−54.3	14.4	11.8	−53.3	6.0	−.21	−18.4	Y	N
V627 Cas	22 55 38.0	+ 58 33 12.0	11.3	−49.8	5.7	8.8	−49.7	10.4	−.12	−2.11	Y	Y
R Peg	23 4 8.0	+ 10 16 24.0	17.6	21.8	5.8	17.2	25.9	10.6	−.99	−2.07	Y	Y
V Cas	23 9 31.0	+ 59 25 42.0	<2			<6			−1.09		N	Y
W Peg	23 17 22.0	+ 26 0 18.0	<2			20.7	−18.1	4.8	−.91	−2.16	Y	Y
S Peg	23 18 1.0	+ 8 38 42.0	<2			<9			−1.11	−2.02	N	Y
RY And	23 18 13.0	+ 39 20 48.0	3.7	0.5	1.7	<7			−.79	−1.98	Y	
BU And	23 21 15.0	+ 39 27 12.0	<2			58.9	−4.8	2.4	−.89	−2.04	Y	
IRC+10537	23 31 15.0	+ 6 1 24.0	<2			<8			−.86	−1.88	Y	
LP And	23 32 .0	+ 43 16 18.0	<2			<7			−.78	−1.56	N	Y
R Aqr	23 41 14.0	− 15 33 42.0	-			310	−27.9	1.7	−1.16	−2.28	N	Y
PZ Cas	23 41 39.0	+ 61 30 42.0	5.8	−41.8	7.9	<7			.07	−1.54	Y	N
EY And	23 42 32.0	+ 43 38 48.0	<2			<8			−.32	−1.95	Y	Y
V657 Cas	23 49 39.0	+ 61 32 31.0	<2			<6			−.40	−1.89	Y	
RS And	23 52 50.0	+ 48 21 36.0	<2			<7			−.86	−1.97	Y	
R Cas	23 55 51.6	+ 51 6 36.4	5.5	26.1	4.0	88.1	25.1	3.6	−.96	−1.84	Y	Y

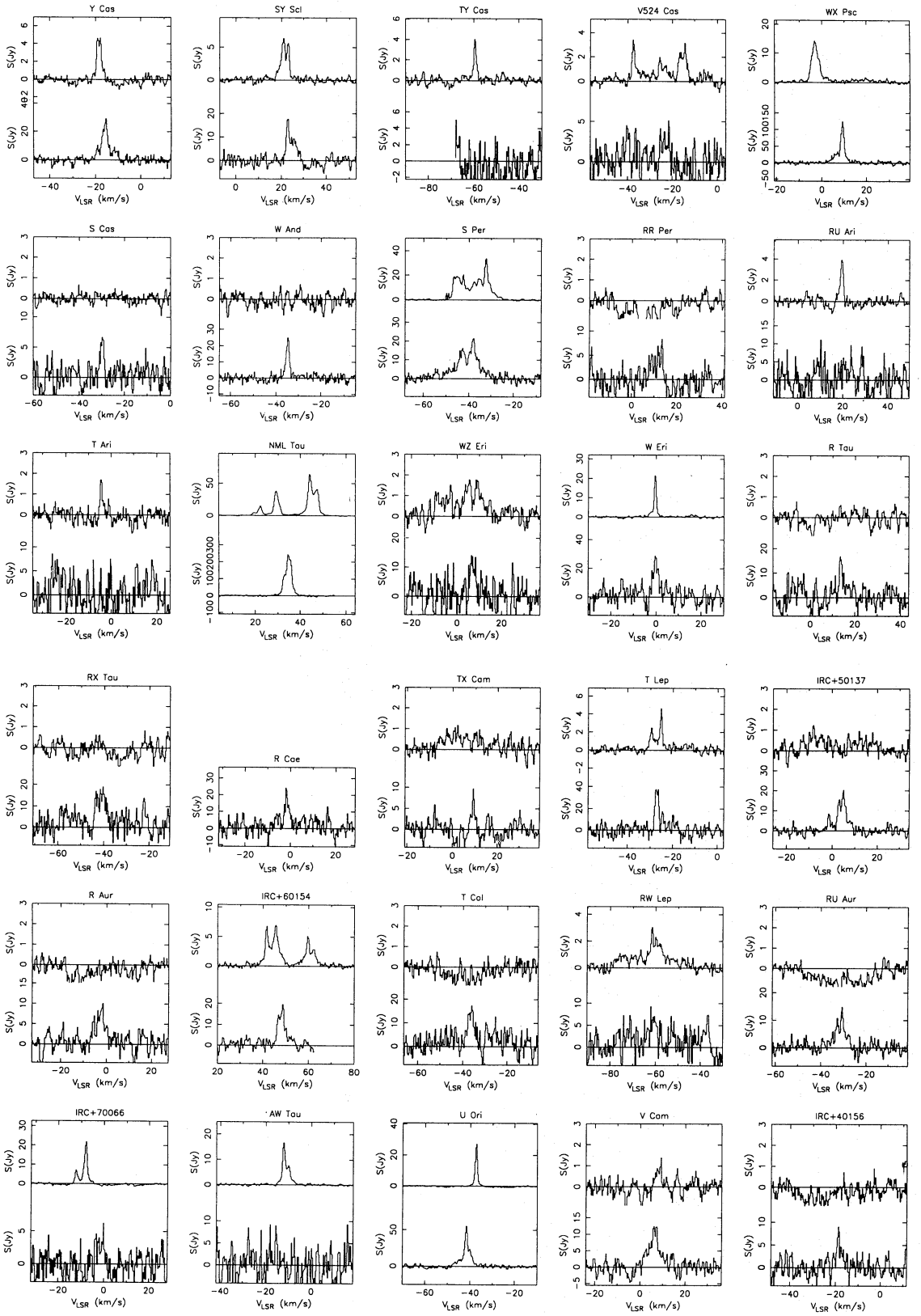

Fig. 1. Line profiles for the H_2O (upper) and SiO($J = 1$–0, $v = 1$) (lower).

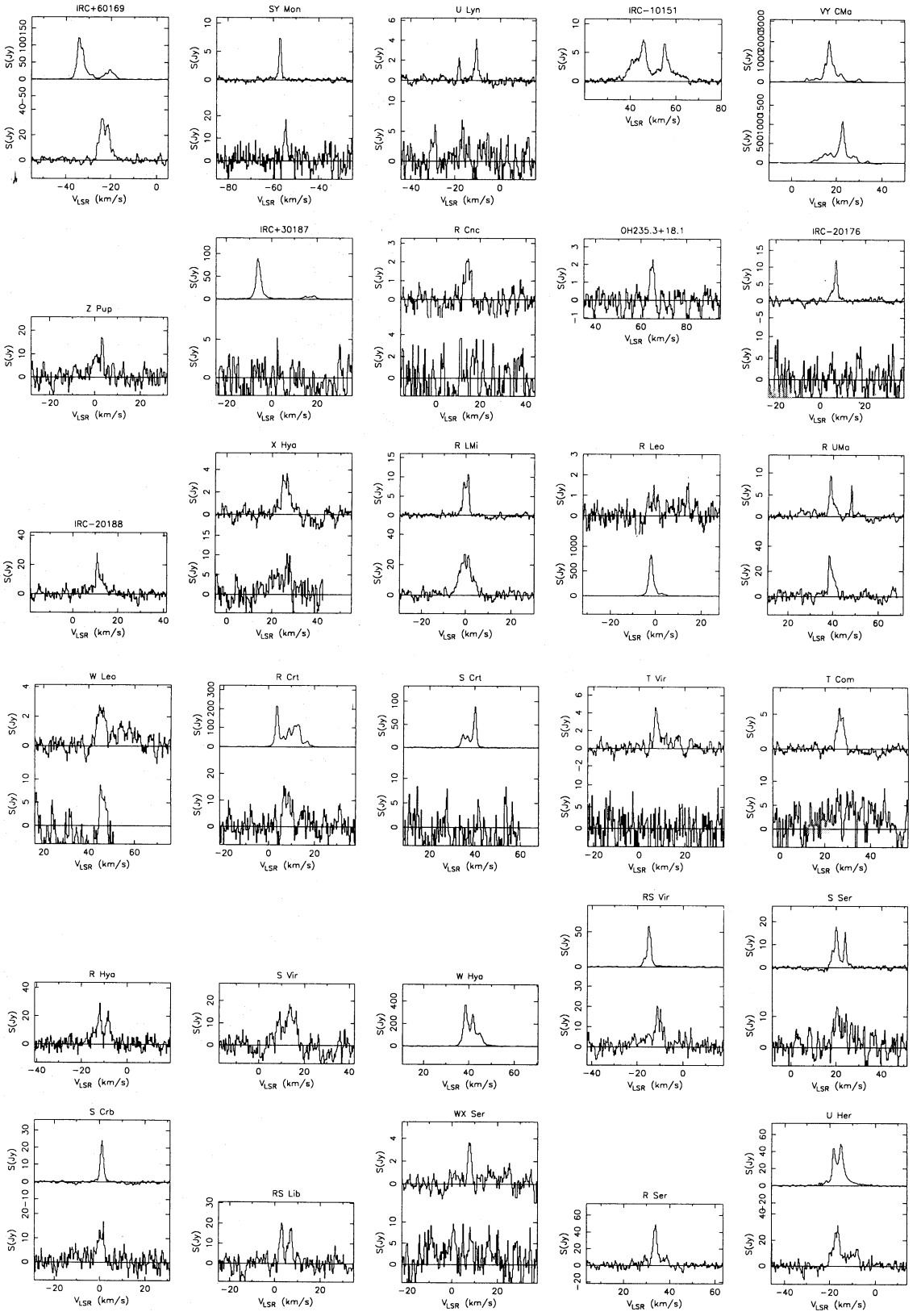

Fig. 1. (continued)

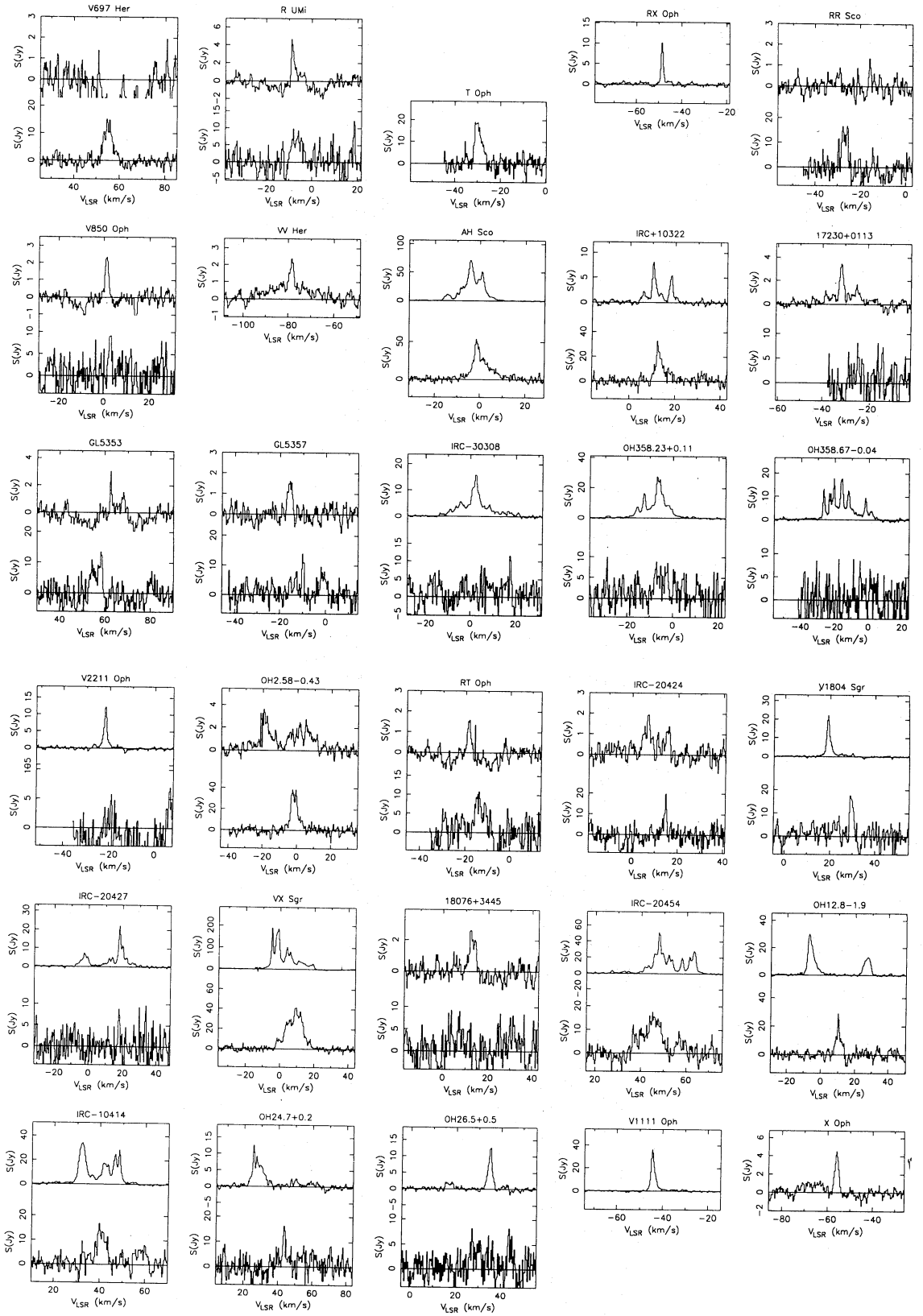

Fig. 1. (continued)

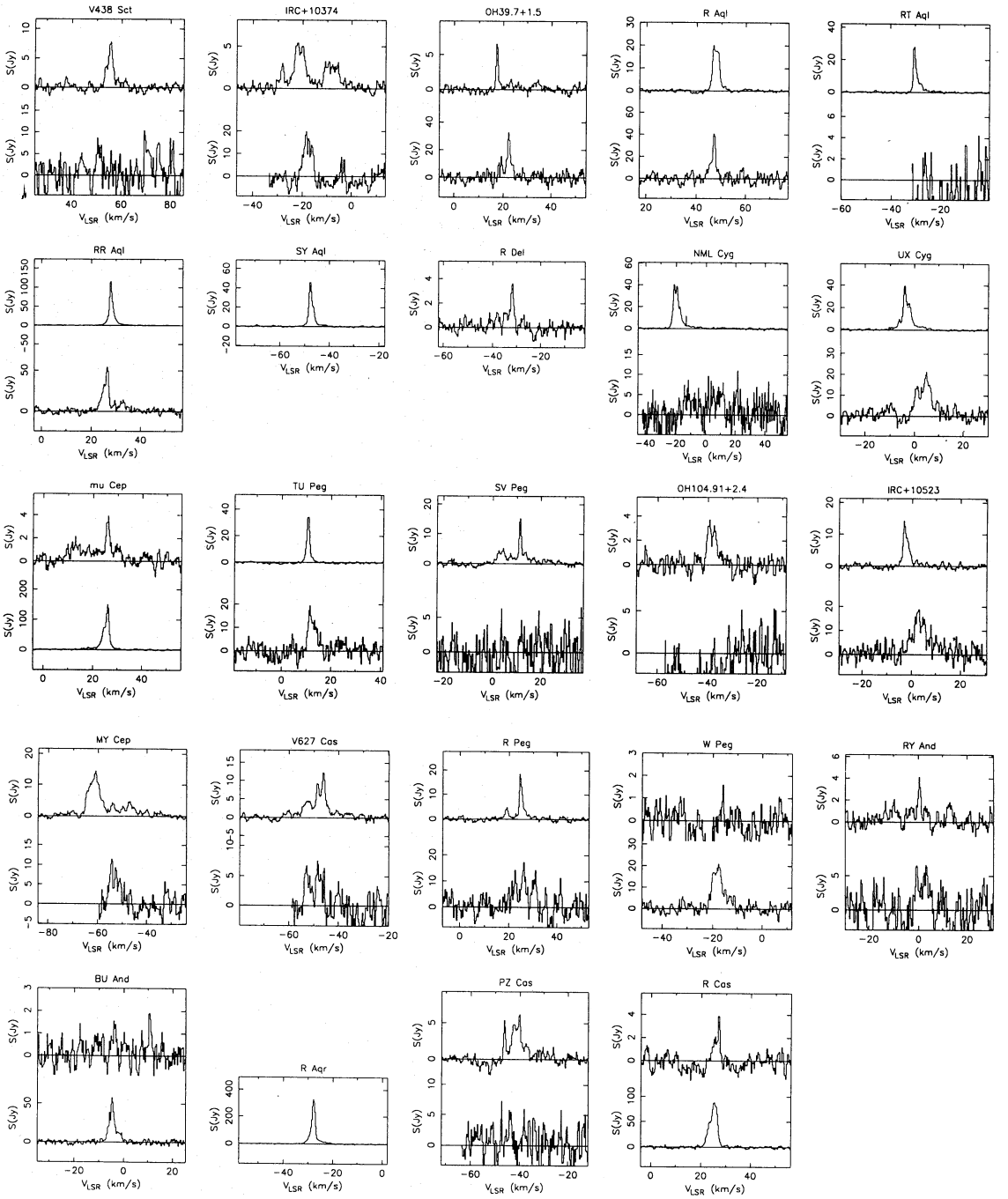

Fig. 1. (continued)

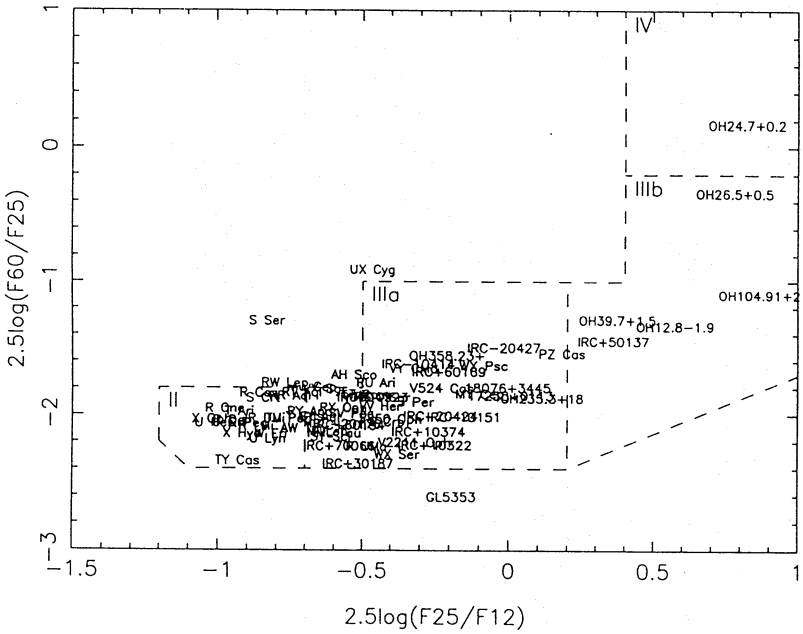

Fig. 2. IRAS two-color diagram of the sources with H_2O masers. The dashed lines are from van der Veen and Habing (1988).

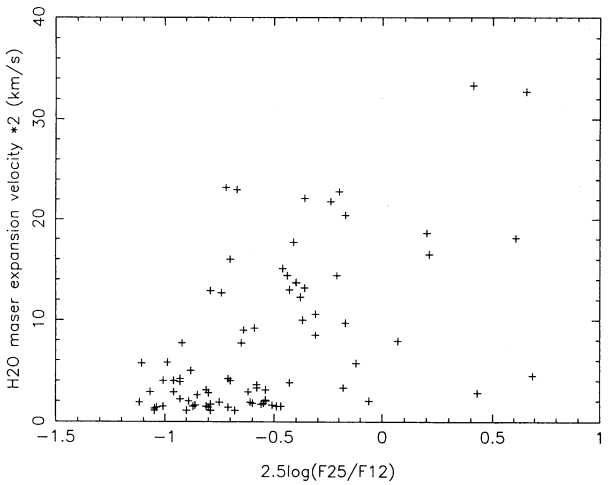

Fig. 3. Expansion velocity obtained from H_2O masers versus the logalithmic ratio of IRAS 12 and 25 μm intensities.

velocity difference.

Jewell et al. (1991) investigated the velocity difference between an OH maser and a SiO ($J = 1$–0, $v = 1$) maser for about 100 stars, and concluded that the SiO maser velocity is a good reference for the stellar velocity. In addition, our results show that in most cases (except for UX Cyg) the H_2O velocities in the Mira variables are also good references for the stellar velocities.

Figure 4 shows IRAS color-color diagrams for all of the sources with both H_2O/SiO masers detected (cross) and the sources with only the SiO maser and no H_2O maser (filled square). In figure 4, sources with both H_2O and SiO masers are the Mira variables (II), IRC/AFGL objects (IIIa), and OH/IR stars (IIIb and IV). However, most of the sources with only a SiO maser are Mira variables; the sources tend to have a small 2.5 log(F25/F12) value (hot color temperature) and are scattering in 2.5 log(F60/F25). The non-detection of H_2O masers might suggest that the sources are in the earliest phases of mass loss, as discussed by Lewis (1989). SiO masers in Mira variables have time variations in phase with the optical or infrared intensity. Our observations of SiO and H_2O were made almost simultaneously. As a result, the detected SiO masers showed that the sources were nearly at the maximum intensities. The non-detection of H_2O masers should thus be the intrinsic characteristics of the sources. Accordingly, this scattering on the IRAS color-color diagram of the SiO maser sources without H_2O must indicate some differences in the physical characteristics of the circumstellar dust/gas envelopes. In addition, we have also plotted all of the sources cataloged by Benson et al. (1990) in the color-color diagrams in figure 5, as in figure 4. Since their observations of H_2O and SiO masers were not simultaneous, their exist some IRC/AFGL and OH/IR sources with a SiO maser but no H_2O maser. However, we

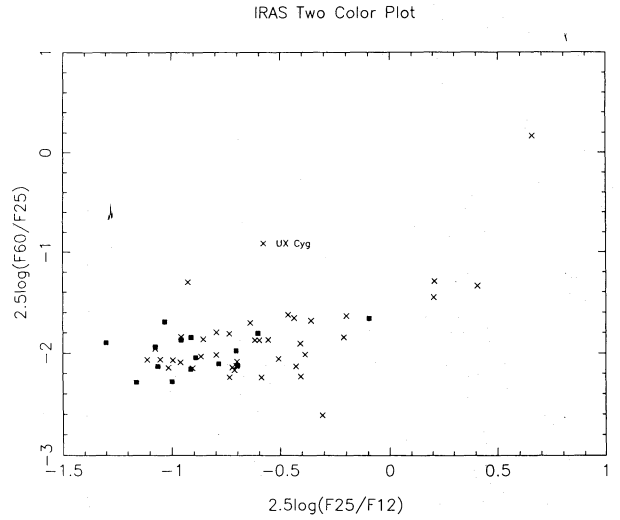

Fig. 4. IRAS two-color diagram of stars with both H_2O and SiO masers (cross), and stars with SiO and no H_2O masers (filled square).

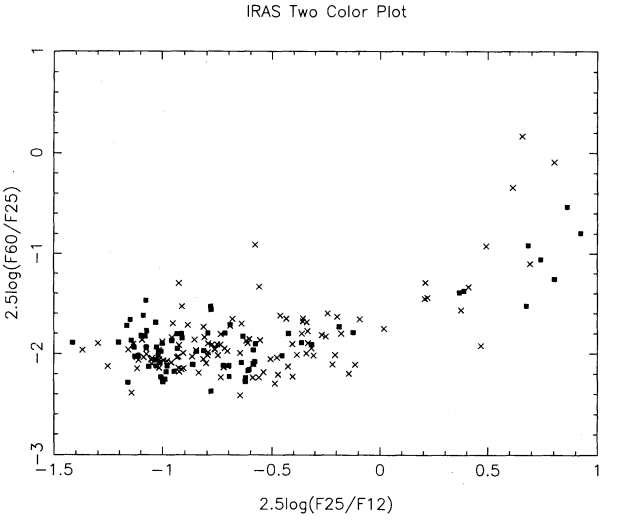

Fig. 5. Same as figure 4 for stars which were cataloged by Benson et al. (1990).

found the same tendency in the region of Mira variables [2.5 log(F25/F12)< −0.5]; those sources with only a SiO maser had a smaller 2.5 log(F25/F12) value and were scattering in 2.5 log(F60/F25). The simultaneous observations should thus be more important for investigating the characteristics of maser emitting stars.

4. Discussion

4.1. Excitation and Beaming Models of the H_2O Maser

The collisional excitation model of the H_2O maser around late-type stars was first proposed by Deguchi (1977). Based on the collisional excitaion model, Cooke and Elitzur (1985) calculated that the location of the 22 GHz H_2O maser emitting region changes at the mass-loss rate. According to their model, the 22 GHz H_2O maser (6_{16}–5_{23}) cannot be observed when the H_2O (6_{16}) in the dense region decays by the radiative process (6_{16}–5_{05}).

A mass loss occurs from the surface of the star. The gas motion around the star is probably highly random, because infall motion also occurs after shock-wave propagation. If the masers are exciting in the hottest gas, they should be emitting from the thin shell surrounding the star. In such a condition, the masers would be beamed in the limb direction, because the optical depth of the line becomes the maximum. In the outer part of the envelope where the temperature is lower than 1500 K, dust forms and the gas starts expanding due to the radiation pressure on grains. The acceleration terminates when the density decreases and the gas-expansion velocity becomes constant, as is observed in the OH and CO spectra.

In Mira variables, SiO and H_2O masers are formed in the closer regions, i.e., within several stellar radii of the star. The SiO and H_2O masers are the tangentially beamed and the velocities coincide with the stellar velocity. Lane et al. (1987) showed a ring-like distribution of low-velocity H_2O maser spots around IK Tau. Using the VLA, Reid and Menten (1990) showed a ring-like distribution of H_2O masers around W Hya, which are explained by limb directional beaming. Recent VLBI observations of SiO masers also show ring-like distributions of maser spots (e.g., Miyoshi et al. 1993 in μ Cep).

In AFGL/IRC objects and OH/IR stars, SiO masers still arise from the inner regions, i.e., stellar photosphere, because they require high temperatures for excitation. In their cases the radial velocity of SiO also coincides with the stellar velocity. However, the H_2O maser in IRC/AFGL objects and OH/IR stars is emitted from the outer region, and the radius of the maser-emitting region increases with the evolutionary sequence of the star. In IRC/AFGL objects, the H_2O maser results from the expanding shell, and should be conically beamed, producing a doubly peaked spectra. In OH/IR stars in which the H_2O maser results from shells with almost a constant expansion velocity, the maser is beamed in the radial direction (like the OH maser), producing double-peak spectra.

This systematic change in the H_2O maser spectra with an evolutionary sequence a strong evidence for the collisional excitation of the H_2O maser in late-type stars.

4.2. Blocking Model of the H_2O Maser Spectra

From the spectra shown in figure 1, we found in IRC/AFGL objects and OH/IR stars in which the blue-shifted peak is likely to be stronger than the red-shifted peak. Especially, some sources (WX Psc, IRC +70066, OH 24.7 − 0.2, V1804 Sgr, IRC +30187, and NML Cyg) show a very weak red-shifted peak. Figure 6 shows the intensity ratio distribution between the red-shifted and blue-shifted emission for the H_2O maser, which has separated peaks and a cold IRAS color [2.5 log(F25/F12)> −0.8]. We took the SiO maser velocity as the reference for sources with both H_2O and SiO masers and calculated the integrated intensities for the blue- and red-shifted components. For sources with only the H_2O maser (IRC +30187, IRC −20427, and OH 26.5 + 0.5), we took the mid-point of the prominent double peaks as the reference velocity. Although it has a prominent blue-shifted peak, we excluded NML Cyg (it was well known as a supergiant star) from figure 6 because it was not observed by the IRAS. Those sources with a stronger blue-shifted peak with more than a factor 2 were 12, whereas the stronger red-shifted peak with more than factor 2 were only 3.

Considering the beaming model presented in the previous section, the intensity difference between the two peaks, which results from the near and far sides of the star, might be explained by the blocking effect of the central star.

Another explanation is maser amplification of the radio continuum emission from the central star at the near side of the maser shell. Sivagnanam et al. (1988) observed some OH maser sources in Mira variables with VLBI, and found that the red-shifted components were resolved out, whereas the blue-shifted components had large correlation amplitudes, indicating the small size of the maser emitting region. They proposed the idea of amplification of the stellar radio continuum. Because the mass-loss rate of the Mira variables is by one or two orders of magnitude lower than those of IRC/AFGL objects and OH/IR stars, the radius of the OH-emitting region in Mira variables is thought to be almost the same as the radius of the H_2O maser-emitting region in the IRC/AFGL and OH/IR stars.

In order to determine whether the asymmetry of the red- and blue-shifted peaks of the H_2O masers is the result of blocking the red-shifted peak, or amplification of the background stellar continuum, VLBI observations should be carried out. We conducted VLBI observations of W Hya and IRC +60169 using Kashima's 34 m telescope, and Nobeyama's 45 m telescope and obtained larger fringe amplitudes for the blue-shifted peak of the H_2O maser than for the red-shifted peak (Takaba et al. 1994). In the future single-dish monitoring of the maser spectra should be made. The intensity of the red-shifted peak varies as the star oscillates if the blocking model is correct. Also, the intensity of the blue-shifted peak may increase with the stellar luminosity for non-saturated maser sources if the amplification model is correct.

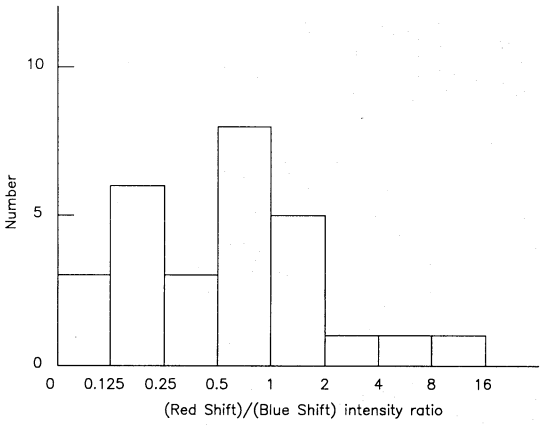

Fig. 6. Number distribution of the (Red-shifted)/(Blue-shifted) integtrated intensity ratio for H_2O maser sources with separated peaks.

In addition, if the blocking model is correct, we can investigate circumstellar physical conditions by observing the scintillations of the red-shifted peak because they pass the region closer to the mass-losing surface of the star.

5. Conclusions

We found that the expansion velocity of the H_2O maser in M-type stars increases with the star evolutionary sequence. The systematic spectral change of the H_2O maser is explained by the shock excitation model proposed by Cooke and Elitzer (1985). The H_2O maser in the Mira variables comes from almost the same region as the SiO maser emitting region, and is also a good indicator of the stellar systemic velocity.

Some H_2O maser sources in IRC/AFGL and OH/IR stars show prominent blue-shifted peaks, that are caused by either blocking of the red-shifted component or amplification of the stellar continuum. Very precise VLBI mapping observations or single-dish monitoring observations are necessary to determine which hypothesis is correct.

We would like to thank all of the people in the Radio Astronomy Applications Section of the Communications Research Laboratory and the VLBI group of the Nobeyama Radio Observatory for their support.

Reference

Alcorea J., Bujarrabal V., Gomez-Gonzalez J. 1990, A&A 231, 431

Bedjin P.J. 1987, A&A 186, 136

Benson P.J., Little-Marenin I.R., Woods T.C., Attridge J.M., Blalis K.A., Rudolph D.B., Rubiera M.E., Keefe H.L. 1990, ApJS 74, 911

Cooke B., Elitzer M. 1985, ApJ 295, 175

Deguchi S. 1977, PASJ 29, 669

Dickinson D.F., Kleinmann S.G. 1977, ApJL 214, L135

Hall P.J., Wright A.E., Troup E.R., Wark R.M., Allen D.A. 1990, MNRAS 247, 549

Jewell P.R., Snyder L.E., Walmsley C.M., Wilson T.L., Gensheimer P.D. 1991, A&A 242, 211

Lane A.P., Johnston K.J., Bowers P.F., Spencer J.H., Diamond P.J. 1987, ApJ 323, 756

Lewis B.M. 1989, ApJ 338, 234

Miyoshi M., Morimoto M., Kawaguchi N., Ukita N., Inoue M., Miyazawa K., Tsuboi M., Miyaji T. et al. 1993, PASJ 44, L259

Netzer N., Knapp G.R. 1987, ApJ 323, 734

Olnon F.M., Baud B., Habing H.J., de Jong T., Harris S., Pottasch S.R. 1984, ApJL 278, L41

Reid M.J., Menten K.M. 1990, ApJL 360, L51

Reid M.J., Moran J.M. 1981, ARA&A 19, 231

Reid M.J., Muhleman D.O., Moran J.M., Johnston K.J., Schwartz P.R. 1977, ApJ 214, 60

Schwartz P.R., Harvey P.M., Barrett A.H. 1974, ApJ 187, 491

Sivagnanam P., Diamond P.J., Squeren A.M.Le., Daigne G., Biraud F., Ortega-Molina A., Graham D.A. 1988 A&A 194, 157

Takaba H. 1991, J. Comm. Res. Lab. 38, 417

Takaba H., Iwata T., Miyoshi M., Ukita N., Kameno S., Matsumoto K. 1994, in Astronomy with Millimeter and Submillimeter Wave Interferometry, IAU Colloquium 140, ASP Conference Series, Vol. 59, ed M. Ishiguro, Wm. J. Welch p62

van der Veen W.E.C.J., Habing H.J. 1988, A&A 194, 125